Nonlinearly coupled vibrational modes and self-trapped states: Single-vibron-oscillator case with α-helix parameters

H. Keith McDowell
CLS-2 MS G738, Los Alamos National Laboratory, Los Alamos, New Mexico 87545

A. M. Clogston
CMS MS K765, Los Alamos National Laboratory, Los Alamos, New Mexico 87545
(Received 11 October 1991; revised manuscript received 2 March 1992)

Quantum molecular-time-scale generalized-Langevin-equation (MTGLE) theory is applied to calculate spectral linewidths and redshifts of a single vibron oscillator nonlinearly coupled by the Davydov Hamiltonian in the α-helix parameter regime to a chain of linearly coupled molecules. Exact values can also be calculated for this problem. The MTGLE theory gives very accurate results for linewidths and less accurate but acceptable results for redshifts over a wide range of temperatures from 10 to 300 K. These results successfully extend previous calculations carried out in the L-alanine parameter regime to the α-helix parameter regime with a 30-fold increase in frequency of the vibron oscillator and a 1000-fold increase in the square of the nonlinear coupling constant. In constrast to the L-alanine case, the vibron-oscillator frequency is more than 16 times greater than the largest frequency in the phonon manifold.

I. INTRODUCTION

One of the most important questions for molecular crystals comprised of two or more nonlinearly coupled vibrational systems is the formation of localized states and their lifetimes. The possibility of such localized states was brought into prominence by Davydov and Kislukha in several papers[1-3] where they proposed that such states might exist on one-dimensional molecular chains, such as the α-helix, because of the interaction of the intramolecular carbon-oxygen amide I stretching modes with low-frequency acoustic phonons. In subsequent work these localized states have become known as vibron solitons.[4] As we described in the first paper in this series (hereafter denoted as I),[5] many efforts have been made theoretically to demonstrate the existence of vibron solitons; however, a survey of this theoretical work shows that disagreement abounds. The experimental situation is little better with only the work of Careri *et al.* on acetanilide cited as proof of their existence.[6] Even the interpretation of this experiment has been challenged.[7-11] Others have suggested that vibron solitons may be present in systems such as L-alanine where libronic degrees of freedom are coupled nonlinearly to phonon degrees of freedom.[12]

The widespread disagreement and confusion as to the existence of vibron solitons points to the need for a systematic theoretical approach for studying such problems. In paper I we introduced the use of quantum molecular-time-scale generalized-Langevin-equation (MTGLE) theory[13,14] as a systematic way of computing the spectral linewidth (or lifetime) of vibron solitons. This theoretical approach is reviewed briefly in Sec. II. In order to test MTGLE theory and to gain insight into the vibron-soliton problem, we chose in I to examine a simpler Hamiltonian system than that used by Davydov,[3] namely, the case of a single oscillator, hereafter referred to as the vibron, coupled to a chain of oscillators constituting a phonon bath. This Hamiltonian does not display solitonic behavior because the longitudinal symmetry of the chain is already broken by the presence of the localized vibron, but is nevertheless an important test case. Specifically, we used the Hamiltonian

$$H=\sum_{k=-N}^{N}\hbar\omega_k(a_k^{\dagger}a_k+\tfrac{1}{2})+\hbar\omega_0(c^{\dagger}c+\tfrac{1}{2}) -(2c^{\dagger}c+1)\sum_{k=-N}^{N}\hbar\sigma_k(a_k+a_k^{\dagger}) , \tag{1}$$

where $c^{\dagger}$ (c) is the creation (annihilation) operator associated with the single vibron oscillator with uncoupled frequency ω_0, $a_k^{\dagger}(a_k)$ is the creation (annihilation) operator for the phonon oscillator of frequency ω_k, and σ_k is given by

$$\sigma_k=\frac{2\bar{\chi}}{\hbar}\mathrm{sgn}k\cos\left[\frac{\pi k}{2N+1}\right]\left[\frac{\sin[\pi k/(2N+1)]}{2N+1}\right]^{1/2} , \tag{2}$$

where $\bar{\chi}$ is the nonlinear coupling parameter expressed in energy units, $2N+1$ is the size of the oscillator chain, which will be taken indefinitely large, and sgn$k$ is the sign ($+1$ or -1) of the index k. The single vibron oscillator is located at site 0, the center of the chain. The dispersion of the phonon-oscillator frequency ω_k is given by

$$\omega_k=\omega_a\left|\sin\frac{\pi k}{2N+1}\right| . \tag{3}$$

As shown by others,[15-17] the Hamiltonian in Eq. (1) is particularly useful to study since it can be exactly diagonalized. We have shown in I that this also allows one to compute analytic results for required MTGLE expressions, and it therefore serves as an excellent testing ground for MTGLE theory while yielding information on

the vibron-soliton question. A summary of the exact theory will be given in Sec. III.

In paper I we carried out a full study of the application of MTGLE theory to Eq. (1) and found that the theory is admirably suited for tackling the Davydov single-vibron-oscillator system in a parameter regime suitable to L-alanine in which the single-vibron-oscillator frequency ω_0 ranged from $0.5\omega_a$ to $1.5\omega_a$. In particular, we focused on the oscillation frequency and spectral linewidth (or lifetime) of the time correlation function

$$\dot{\chi}(t)=\tfrac{1}{2}\langle[c(t),c^{\dagger}(0)]+[c(0),c^{\dagger}(t)]\rangle \ , \tag{4}$$

where the brackets $\langle\cdots\rangle$ represent a quantum-statistical canonical ensemble average. The spectral density of $\dot{\chi}(t)$ is denoted by $\rho(\omega)$ and is given by

$$\rho(\omega)=\frac{2}{\pi}\int_0^{\infty}dt\,\dot{\chi}(t)\cos\omega t \ . \tag{5}$$

If we invert Eq. (5), we have

$$\dot{\chi}(t)=\int_0^{\infty}d\omega\,\rho(\omega)\cos\omega t \ , \tag{6}$$

and it is then easy to show that

$$\left[\left[\frac{d}{dt}\right]^{2n}\dot{\chi}(t)\right]_{t=0}=(-1)^n\int_0^{\infty}d\omega\,\omega^{2n}\rho(\omega) \ , \tag{7}$$

so that the derivatives of $\dot{\chi}(t)$ at $t=0$ are simply related to the moments of $\rho(\omega)$. For the parameter domain assumed in I, $\rho(\omega)$ represented a single redshifted line characterized by a maximum frequency $\omega_{\max}$ and a linewidth $\Delta\omega$ related, respectively, to the oscillation frequency and lifetime of $\dot{\chi}(t)$. There is no requirement in the theory that the line shape be symmetric or Lorentzian in shape.

As summarized in I, with more complete details provided in a subsequent paper,[17] we have extended previous work on the exact theory to obtain exact expressions for $\dot{\chi}(t)$ and $\rho(\omega)$. This allowed extensive comparisons of MTGLE theory with exact results. In particular, the position of the maximum of $\rho(\omega)$ calculated by MTGLE theory was in excellent agreement with results of the exact theory and could be accurately represented by the formula

$$\omega_{\max}=\omega_0-[2n(\omega_b)+1]8\eta \ , \tag{8}$$

derived from the exact theory. In this expression

$$n(\omega)=\left[\exp\left[\frac{\hbar\omega}{kT}\right]-1\right]^{-1} \ , \tag{9}$$

$$\omega_b=\omega_0-4\eta \ , \tag{10}$$

and

$$\eta=\sum_k\frac{\sigma_k^2}{\omega_k}=\frac{2\bar{\chi}^2}{\hbar^2\omega_a} \ . \tag{11}$$

The constant k is Boltzmann's constant, and T is the absolute temperature. In addition, the oscillation frequency of $\dot{\chi}(t)$ was in good agreement with the exact result over the valid time domain of MTGLE theory and was accurately represented by $\omega_{\max}$ given by Eq. (8). Furthermore, the lifetime τ calculated by MTGLE theory was in agreement for temperatures greater than about 2 K with the exact lifetime given by

$$\tau=\frac{\omega_a^2\hbar^3}{32kT\bar{\chi}^2} \tag{12}$$

and obtained from the exact theory as described in the next section. As shown elsewhere,[18] the spectral density $\rho(\omega)$ is related to the dipole spectrum of the system, so that knowledge of one is equivalent to knowledge of the other.

In this paper we extend our study of the single-vibron-oscillator case to the parameter regime appropriate to the α-helix. We chose the values $\hbar\omega_0=1665\ \mathrm{cm}^{-1}$, $\hbar\omega_a=100\ \mathrm{cm}^{-1}$, and $\bar{\chi}=10\ \mathrm{cm}^{-1}$, which are typical of values assumed in the literature. As will be noted later, compared to the L-alanine system, for the α-helix system ω_0 has been increased by a factor of approximately 30 and the square of the coupling constant by a factor of more than 1000. As will be seen in the following sections, we find that MTGLE theory with a limited number of moments of $\dot{\chi}(t)$ continues to make accurate predictions of relaxation time and satisfactory predictions of the redshifted frequency $\omega_{\max}$ even under these extreme conditions. The main difference is that the moments must be calculated to higher order in the coupling constant to obtain the best agreement between MTGLE and the exact theories.

The paper is organized as follows: In Sec. II we review the essential features of MTGLE theory as required for the discussion of the results of calculations in the α-helix parameter regime. Section III will summarize the exact theory and give the exact expressions for $\dot{\chi}(t)$ needed for comparison with MTGLE theory. Section IV will present results for α-helix parameters including comparison with exact theory. Section V will contain some discussion and concluding remarks.

II. REVIEW OF MTGLE THEORY

MTGLE theory is founded on the notion that time correlation functions or their spectral density can be built up from short-time or molecular-time-scale information.[13,14] In particular, we focus on the time correlation function $\dot{\chi}(t)$ given by Eq. (4) and its spectral density given by Eq. (5). The basic information about the quantum system required in MTGLE theory is the short-time derivatives of $\dot{\chi}(t)$ [or moments of $\rho(\omega)$] given by

$$\sigma_0^{(n)}=(-1)^n\left[\left[\frac{d}{dt}\right]^{2n}\dot{\chi}(t)\right]_{t=0}$$
$$=\langle[c^{(n)}(0),c^{(n)\dagger}(0)]\rangle \ , \tag{13}$$

where

$$c^{(n)}(0)=\left.\frac{d^nc(t)}{dt^n}\right|_{t=0} \ . \tag{14}$$

To show how these short-time derivatives are used in MTGLE theory, we first define the Laplace transform of Eq.(4) by

$$\hat{\chi}(z)=\int_0^\infty dt\, e^{-zt}\chi(t) \ . \tag{15}$$

From the Laplace transform $\hat{\chi}(z)$, we create a set of bath functions $\hat{\theta}_m(z)$ such that

$$\hat{\chi}(z)=[z^2+\omega_{e_0}^2-\omega_{c_1}^4\hat{\theta}_1(z)]^{-1} \tag{16}$$

and

$$\hat{\theta}_m(z)=[z^2+\omega_{e_m}^2-\omega_{c_{m+1}}^4\hat{\theta}_{m+1}(z)]^{-1} \ , \tag{17}$$

where

$$\omega_{e_m}^2=\sigma_m^{(1)} \ , \tag{18}$$

$$\omega_{c_{m+1}}^4=\sigma_m^{(2)}-(\sigma_m^{(1)})^2 \ , \tag{19}$$

and

$$\sigma_m^{(n)}=(-1)^n\left[\left[\frac{d}{dt}\right]^{2n}\dot{\theta}_m(t)\right]_{t=0} \ . \tag{20}$$

The constants $\omega_{e_m}^2$ and $\omega_{c_m}^4$ are known as the Einstein and coupling frequencies, respectively. To determine $\hat{\theta}_m(z)$ or equivalently $\theta_m(t)$, we relate the time derivatives in Eqs. (13) and (20) by the equation[5]

$$\sigma_m^{(n)}=\omega_{e_m}^2\sigma_m^{(n-1)}+\omega_{c_{m+1}}^4\sum_{k=0}^{n-2}\sigma_{m+1}^{(k)}\sigma_m^{(n-2-k)} \ . \tag{21}$$

Thus the short-time derivatives $\sigma_m^{(n)}$ of each function $\theta_m(t)$ can be computed in a bootstrap process from the preceding set of moments $\sigma_{m-1}^{(n)}$. In what follows we refer to the index m as the bath index. The inverse Laplace transform of Eq. (16) gives an expression for $\dot{\chi}(t)$ in terms of the first bath function $\theta_1(t)$,

$$\frac{d^2}{dt^2}\dot{\chi}(t)=-\omega_{e_0}^2\dot{\chi}(t)+\omega_{c_1}^4\int_0^t d\tau\,\theta_1(t-\tau)\dot{\chi}(\tau) \ . \tag{22}$$

To make use of the constants $\sigma_m^{(n)}$, we have developed in I a fitting scheme for the first bath function $\theta_1(t)$. We expand $\theta_1(t)$ in a set of GLE functions $G_k(t)$ such that

$$\theta_1(t)=\sum_k \alpha_k G_k(t) \ , \tag{23}$$

where

$$G_k(t)=\frac{1}{\pi}\int_0^\pi dx[\cos(k-1)x-\cos(k+1)x]\frac{\sin\Omega t}{\Omega} \tag{24}$$

and

$$\Omega=(\omega_e^2-2\omega_c^2\cos x)^{1/2} \ . \tag{25}$$

The expansion constants α_k are determined by matching the derivatives at time zero of Eq. (23) with the constants $\sigma_1^{(n)}$ as defined by Eq. (20). The sum over k in Eq. (23) is finite since we are generally limited for numerical reasons to the first 15–20 derivatives. In Sec. IV we examine the convergence of MTGLE results as a function of the number of GLE functions used in Eq. (23). We refer to the maximum index used in Eq. (23) as the GLE index k. In particular, we assume that n time derivatives of $\dot{\theta}_1(t)$ are known so that the Einstein and coupling frequencies in Eqs. (18) and (19) can be computed to bath index $N=(n+1)/2$ (not to be confused with the large number $2N+1$ of oscillators in the chain). With this convention the maximum possible value for k is $2N=n+1$.[5] The number n of time derivatives of $\theta_1(t)$ is always 2 less than the number of time derivatives of $\dot{\chi}(t)$.

From Eq. (25) we see that two parameters ω_e and ω_c remain to be determined. If we define the exact spectral density $\rho_1(\omega)$ of the first heat bath by

$$\rho_1(\omega)=\frac{2}{\pi}\int_0^\infty dt\,\dot{\theta}_1(t)\cos\omega t \ , \tag{26}$$

then one can show that the finite expansion for $\theta_1(t)$ in Eq. (23) leads to the following approximation $\rho_1^*(\omega)$ to the exact spectral density $\rho_1(\omega)$; namely,[5]

$$\rho_1^*(\omega)=\frac{2\omega}{\pi\omega_c^2}\sum_{k=1}^{2N}\alpha_k\sin k\phi(\omega) \ , \tag{27}$$

where

$$\cos\phi(\omega)=\frac{\omega_e^2-\omega^2}{2\omega_c^2} \ . \tag{28}$$

As can be seen from Eq. (28), the parameters ω_e and ω_c determine the lower and upper band edges of $\rho_1^*(\omega)$. Alternatively, they can be understood as determining the center frequency and width of $\rho_1^*(\omega)$. In this paper we present a different approach than the one used in I to compute ω_e and ω_c. The details are given in the Appendix. The new approach is more robust and eliminates the undesired oscillatory behavior of $\rho_1^*(\omega)$ sometimes found in I. As noted in the Appendix, this approach results in a more uniform representation of $\rho_1^*(\omega)$ in the sense defined by Levine[19] and, therefore, in a spectral density of larger entropy consistent with the set of n moments specified in Eq. (27) independent of the values of ω_e and ω_c.

Having obtained suitable values for ω_e and ω_c, $\theta_1(t)$ and $\hat{\theta}_1(z)$ are determined and can be used to determine $\rho(\omega)$ in Eq. (5). We note first that

$$\rho(\omega)=-\frac{2\omega}{\pi}\mathrm{Im}\hat{\chi}(i\omega) \ . \tag{29}$$

But from Eq. (16), we have that

$$\hat{\chi}(i\omega)=[\omega_{e_0}^2-\omega^2-\omega_{c_1}^4\hat{\theta}_1(i\omega)]^{-1} \ . \tag{30}$$

Defining

$$I(\omega)=\omega_{c_1}^4\mathrm{Im}\hat{\theta}_1(i\omega) \tag{31}$$

and

$$R(\omega)=\omega_{c_1}^4\mathrm{Re}\hat{\theta}_1(i\omega) \ , \tag{32}$$

one can then show using Eqs. (29)–(32) that

$$\rho(\omega)=-\frac{2\omega}{\pi}\frac{I(\omega)}{[\omega_{e_0}^2-\omega^2-R(\omega)]^2+I(\omega)^2} \ . \tag{33}$$

This form for $\rho(\omega)$ and the underlying relationship to $\theta_1(t)$ is the principal result of this section. To find the frequency at the maximum of the peak in Eq. (33), which

we denote by $\omega_{\max}$, we use a computer search subroutine which walks its way to the maximum. In all cases studied to date, this is very close to the solution of the equation $\omega^2-\omega_{e_0}^2+R(\omega)=0$, so that in the following section we will sometimes designate $\omega_{\max}$ as the resonant frequency. Once $\omega_{\max}$ is known, we approximate the lifetime τ by

$$\tau=-\frac{2\omega_{\max}}{I(\omega_{\max})} . \tag{34}$$

In Sec. IV we will present results for $\omega_{\max}$ and τ as a function of temperature using α-helix Hamiltonian parameters. To show the kind of convergence that is obtained as more moments are used, $\omega_{\max}$ and τ will be plotted as a function of the GLE index k up to the highest available value. In these plots the parameters ω_e and ω_c are fixed at the values determined by the fitting described in the Appendix.

III. SUMMARY OF EXACT THEORY

As mentioned in the Introduction, the Hamiltonian in Eq. (1) can be exactly diagonalized by a canonical transformation so that an exact expression can be found for the correlation function $\dot{\chi}(t)$. In McDowell and Clogston,[17] this is given in the form of a product of two factors,

$$\dot{\chi}(t)=f(t)e(t) , \tag{35}$$

where $f(t)$ is an ensemble average over renormalized vibron variables and $e(t)$ is an ensemble average over renormalized phonon variables. The explicit form for $f(t)$ is

$$f(t)=\langle (n+1)\cos[\omega_0-8\eta(n+1)t+g(t)] -n\cos[(\omega_0-8\eta n)t+g(t)]\rangle_D , \tag{36}$$

where $\langle\cdots\rangle_D$ represents the ensemble average over the renormalized vibron variables, n is the corresponding number operator, and $g(t)$ is given by

$$g(t)=\frac{8\eta}{\omega_a}\int_0^{\omega_a t}dx\frac{J_1(x)}{x} \cong\frac{8\eta}{\omega_a} , \tag{37}$$

for $\omega_a t>2\pi$. As shown in McDowell and Clogston,[17] for $\omega_a t>2\pi$, $f(t)$ can be put into the form

$$f(t)=\frac{2\cos(\omega_0 t-2\tan^{-1}\{[2n(\omega_b)+1]\tan 4\eta t\})}{\{1+[2n(\omega_b)+1]^2\}+\{1-[2n(\omega_b)+1]^2\}\cos 8\eta t} . \tag{38}$$

For times much less than $1/8\eta$ and temperatures up to $\hbar\omega_0/k$, $f(t)$ becomes approximately

$$f(t)=\cos\{\omega_0-[2n(\omega_b)+1]8\eta\}t =\cos\omega_{\max}t , \tag{39}$$

with $\omega_{\max}$ defined by Eq. (8).

The explicit form for $e(t)$ is

$$e(t)=\exp\left\{\left[-\frac{8\eta}{\omega_a}\right]\left[h(t)+\frac{2}{\pi}\ln\frac{\hbar\beta}{2\pi t}(1-e^{-2\pi t/\hbar\beta}) +\frac{2t}{\hbar\beta}\right]\right\} , \tag{40}$$

where $\beta=(kT)^{-1}$ and

$$h(t)=\int_0^{\omega_a t}dx\frac{\mathcal{H}_1(x)}{x} \cong 0.172\,118+\frac{2}{\pi}\ln\omega_a t , \tag{41}$$

for $\omega_a t>2\pi$. The function $\mathcal{H}_1(x)$ is a Sturve function.[17] For $2\pi t\ll\hbar\beta$ and $\omega_a t>2\pi$, $e(t)$ can be written

$$e(t)\cong\exp\left\{\left[-\frac{8\eta}{\omega_a}\right]\left[0.172\,118+\frac{2}{\pi}\ln\omega_a t\right]\right\} , \tag{42}$$

which exhibits the nonexponential decay of $\dot{\chi}(t)$ discussed in McDowell and Clogston.[17] For $2\pi t\gg\hbar\beta$,

$$e(t)\cong\exp\left\{\left[-\frac{8\eta}{\omega_a}\right]\left[0.172\,118+\frac{2}{\pi}\ln\frac{\hbar\omega_a\beta}{2\pi}+\frac{2t}{\hbar\beta}\right]\right\} , \tag{43}$$

so that

$$\tau=\frac{\hbar\omega_a\beta}{16\eta} =\frac{\omega_a^2\hbar^3}{32kT\bar{\chi}^2} , \tag{44}$$

as given in Eq. (12).

IV. MTGLE RESULTS AND COMPARISONS WITH EXACT THEORY

In this section we examine MTGLE results for the α-helix parameter regime and compare with the results of the exact theory summarized in Sec. III and more completely by McDowell and Clogston.[17] As a choice of the Hamiltonian parameters, we use the values $\hbar\omega_0=1665$ cm^{-1}, $\hbar\omega_a=100$ cm^{-1}, and $\bar{\chi}=10$ cm^{-1}. The conclusions of this paper are not affected by small changes in these parameters, and we consider them a representative set.

For the purpose of understanding the behavior of MTGLE computations and their relationship to exact results for the α-helix parameter regime, we have carried out two types of MTGLE computations. In the first procedure we compute the constants $\sigma_0^{(n)}$ to fourth order in the parameter $\bar{\chi}$ using the formula given in I. We find that numerical stability is maintained in the bootstrap process defined by Eq. (21) for a starting set of 13 nonzero derivatives of $\dot{\chi}(t)$ corresponding to a maximum bath index of $N=6$. Although derivatives can be computed for $n>13$, rounding errors involved in the inherent

subtractions in Eq. (21) lead to unstable values for $\omega_{e_n}^2$ and $\omega_{c_n}^4$. In addition, for the α-helix parameter regime we have found that another numerical problem separate from the stability problem in Eq.(21) arises; namely, the constants $\omega_{e_n}^2$ and$\omega_{c_n}^4$ can become negative. This problem is related to both the fact that the derivatives computed to fourth order in $\bar{\chi}$ are only approximate and the fact that the Davydov Hamiltonian for vibrons is an approximate Hamiltonian in the sense of the rotating-wave approximation. This approximation destroys the relation $P=m\dot{Q}$, where

$$P=\left[\frac{m\hbar\omega_0}{2}\right]^{1/2}(c+c^{\dagger}) \tag{45}$$

and

$$Q=i\left[\frac{\hbar}{2m\omega_0}\right]^{1/2}(c-c^{\dagger})\,, \tag{46}$$

and can lead to the unphysical result that the spectral density $\rho(\omega)$ has regions in which $\rho(\omega)<0$. We have examined this problem in detail elsewhere.[20] We describe the consequences of this problem as it arises in the following discussions.

In the second procedure we compute the constants $\sigma_0^{(n)}$ to all orders in $\bar{\chi}$ using the computer program described in I. For this case we are limited by the number of constants $\sigma_0^{(n)}$ that can be computed and not by the bootstrap process. This limitation as described in I is due to the rapid increase as n increases in the number of individual terms contributing to $\sigma_0^{(n)}$, which in turn leads to a large demand on computer time. The maximum number of constants which can be computed is 9. This translates to a maximum bath index N of 4 and a maximum GLE index of $k=8$.

For clarity, the following presentation of results calculated in the α-helix regime from MTGLE and the exact theories is organized into four parts: Section IV A will contain results for the lifetime of $\dot{\chi}(t)$ calculated by MTGLE theory from Eq. (34) and by the exact theory from Eq. (12). The lifetime results will be supplemented with plots of the modulus of $\dot{\chi}(t)$, denoted by $|\dot{\chi}(t)|$, versus time to bring out more detail than is conveyed by lifetime alone. Plots of $|\dot{\chi}(t)|$ also bring out the fact that the modulus is only approximately exponential and that the lifetimes given by Eqs. (34) and (12) are therefore only approximate representations of the time decay. Section IV B will present results for the center of the redshifted line, $\omega_{\max}$, calculated from MTGLE and the exact theories. These results will be supplemented with some examples of the complete spectral density curves to bring out the close similarity of the MTGLE and exact results, including the non-Lorentzian shape of the lines. Section IV C will show the time-dependent radian frequency of $\dot{\chi}(t)$ calculated from MTGLE and the exact theories to bring out how closely MTGLE theory reproduces the exact time evolution of $\dot{\chi}(t)$. Finally, Sec. IV D will present some summary curves showing τ and $\omega_{\max}$ as a function of temperature for fourth-order and all-order MTGLE theory and for the exact theory.

In translating the linewidth of the spectral density into a decay time by using the Lorentzian fit in Eq. (34), one should recognize [because the vibron number operator commutes with the Hamiltonian in Eq. (1)] that the excitation of the vibron itself does not decay in time, but is dephased. The linewidth of the spectral density is thus a measure of the decay time of the time correlation function $\dot{\chi}(t)$ due to dephasing of the excitation. In subsequent work, as we include nearest-neighbor interactions between vibrons, the decay of the excitation itself as well as dephasing will occur and be reflected in the behavior of $\dot{\chi}(t)$

A. Lifetime τ and $|\dot{\chi}(t)|$

In Figs. 1–5 we show the relaxation time τ calculated as a function of the GLE expansion index k for fixed values of the parameters ω_e and ω_c and for $T=10$, 50, 100, 200, and 300 K. The parameters for these curves and those that follow are the values given above: $\hbar\omega_0=1665\ \mathrm{cm}^{-1}$, $\hbar\omega_a=100\ \mathrm{cm}^{-1}$, and $\bar{\chi}=10\ \mathrm{cm}^{-1}$. The calculations are carried out for the MTGLE moments calculated both to fourth order and all orders. Figures 1–5 also include the exact lifetimes calculated from Eq. (12). Both procedures numerically converge to approximately the same value, although the procedure which uses exact moments generally converges more rapidly. The converged values of both procedures approximate with the exact values for most temperatures except that agreement of the fourth-order calculation is poor at 10 K. Agreement of the all-orders calculation is particularly good except at the highest temperatures. As mentioned above, this residual disagreement of the all-orders calculation is due to the use of Eq. (34) to extract lifetimes from the MTGLE spectral density. This equation assumes that the line shape for $\rho(\omega)$ is nearly Lorentzian, but as we shall see in the next section, $\rho(\omega)$ is asym-

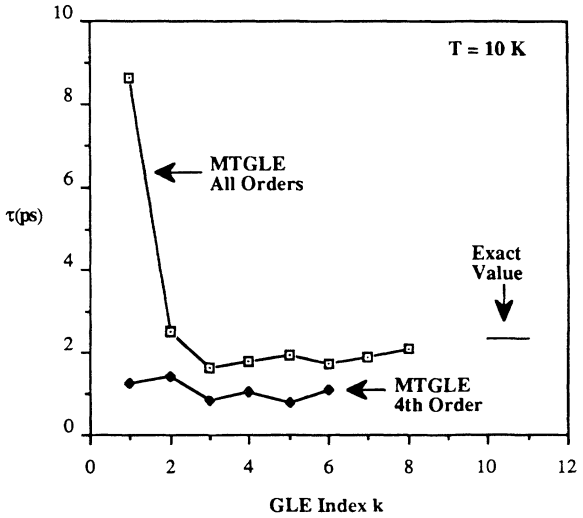

FIG. 1. Relaxation time τ as a function of GLE expansion index k for fixed values of the parameters ω_e and ω_c and $T=10$ K. The Hamiltonian parameters are given in the text. The MTGLE calculations are carried out to fourth order in the coupling constant and to all orders in the coupling constant.

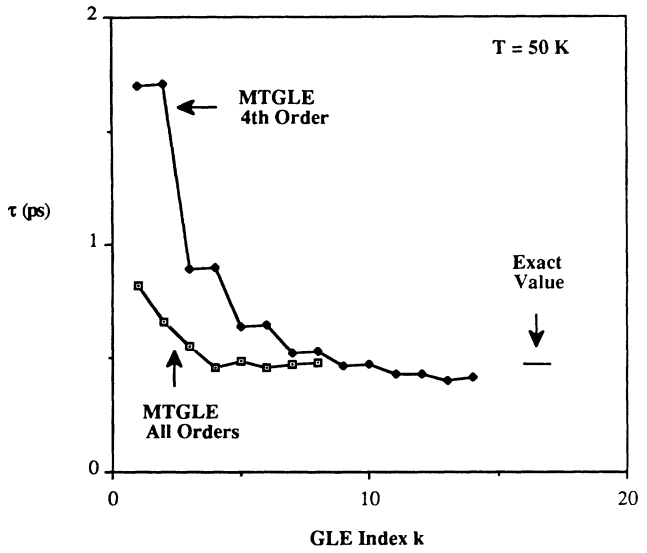

FIG. 2. Same as Fig. 1 with $T=50$ K.

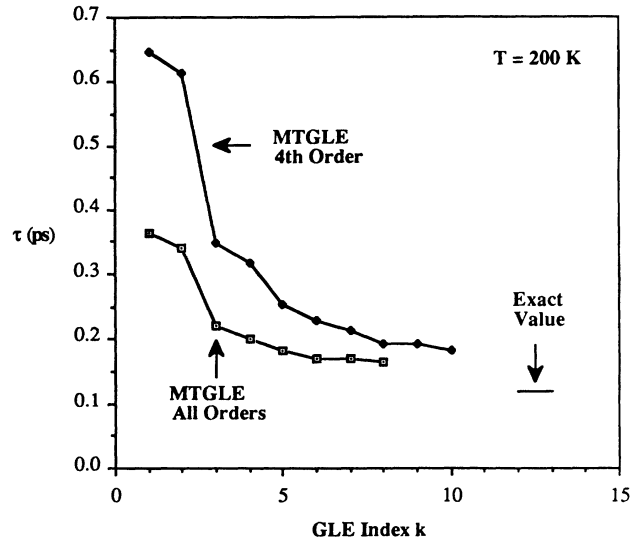

FIG. 4. Same as Fig. 1 with $T=200$ K.

metric, having a pronounced tail on the high-frequency side. In Figs. 6–10 we show the actual decay of $|\dot{\chi}(t)|$ with time for the same temperature range. The MTGLE result in each case uses the highest available GLE index. The exact result is based on Eqs. (35), (36), and (40) in Sec. III. The agreement between the exact result and the MTGLE all-orders calculation is excellent in all cases including the behavior quadratic in t at small times. The fourth-order MTGLE calculation deviates substantially in that it decreases too rapidly at low temperatures and somewhat too slowly at the highest temperatures.

The overall conclusion of this section is that excellent agreement between the exact and MTGLE theories is obtained for the lifetime of $\dot{\chi}(t)$ provided the MTGLE calculation is carried to all orders. If the calculation is carried only to fourth order, agreement is only approximate and considerable disagreement is found at the lowest and highest temperatures and longer times.

B. Spectral density curves and resonant frequency

In Figs. 11–15 we show the resonant frequency $\omega_{\max}$ of the spectral density curves calculated as a function of the GLE expansion index k for fixed values of the parameters ω_e and ω_c and for $T=10$, 50, 100, 200, and 300 K. The parameters for these curves are the same as those assumed in Sec. IV A. The calculations are carried out for the MTGLE moments calculated both to fourth order and all orders. Figures 11–15 also include the exact value of $\omega_{\max}$ calculated from Eq. (8) or the exact expressions for $\dot{\chi}(t)$ given by Eqs. (35), (36), and (40). We note first that the MTGLE all-orders calculations of $\omega_{\max}$ con-

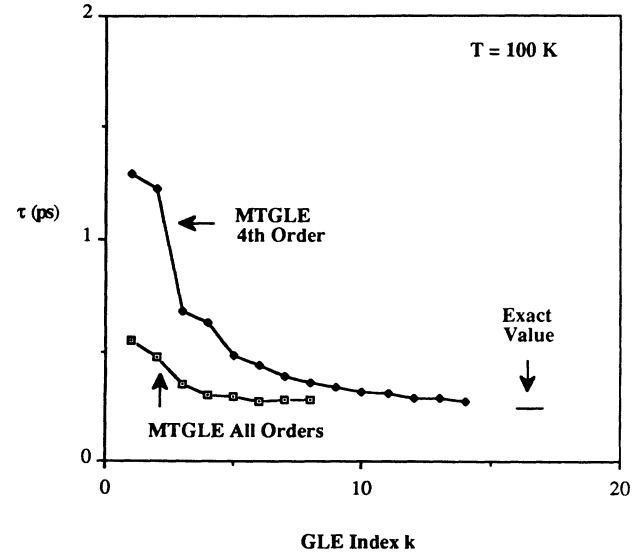

FIG. 3. Same as Fig. 1 with $T=100$ K.

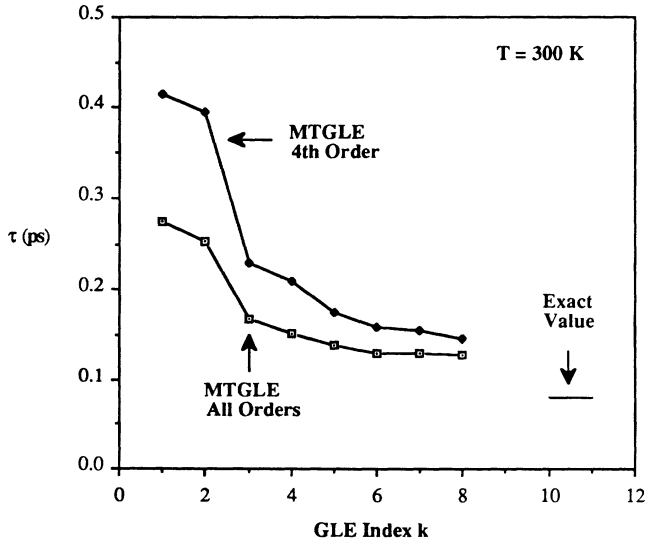

FIG. 5. Same as Fig. 1 with $T=300$ K.

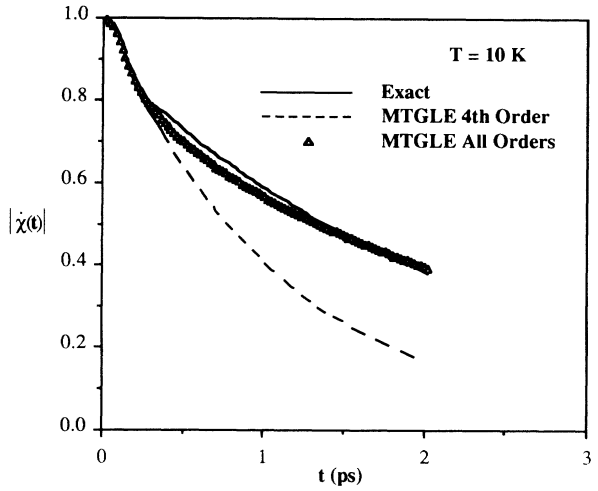

FIG. 6. $|\dot{\chi}(t)|$ as a function of time for $T=10$ K computed from the exact and MTGLE theories. The Hamiltonian parameters are given in the text. The MTGLE calculations are carried out to fourth order and to all orders in the coupling constant.

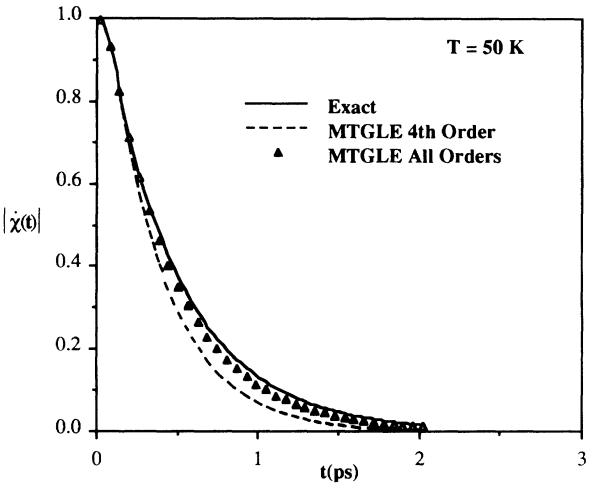

FIG. 7. Same as Fig. 6 with $T=50$ K.

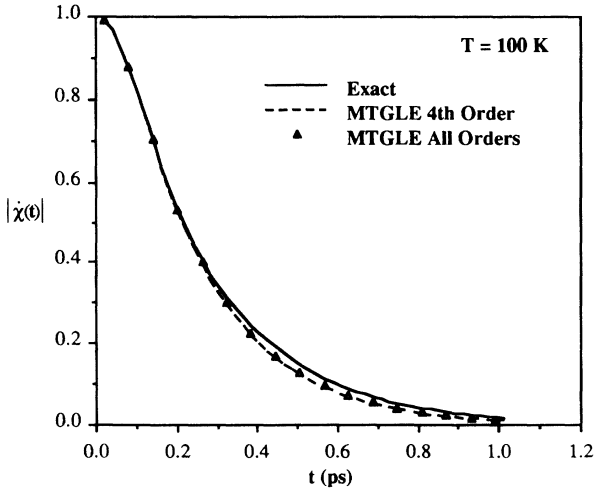

FIG. 8. Same as Fig. 6 with $T=100$ K.

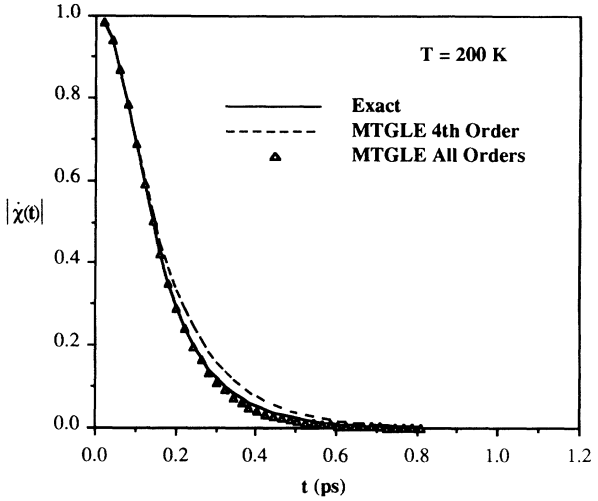

FIG. 9. Same as Fig. 6 with $T=200$ K.

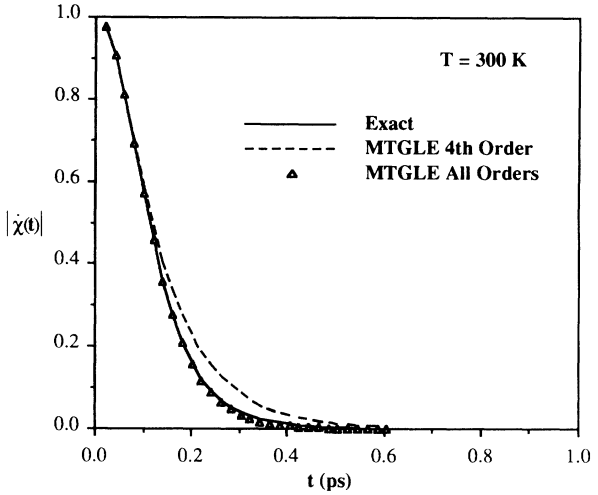

FIG. 10. Same as Fig. 6 with $T=300$ K.

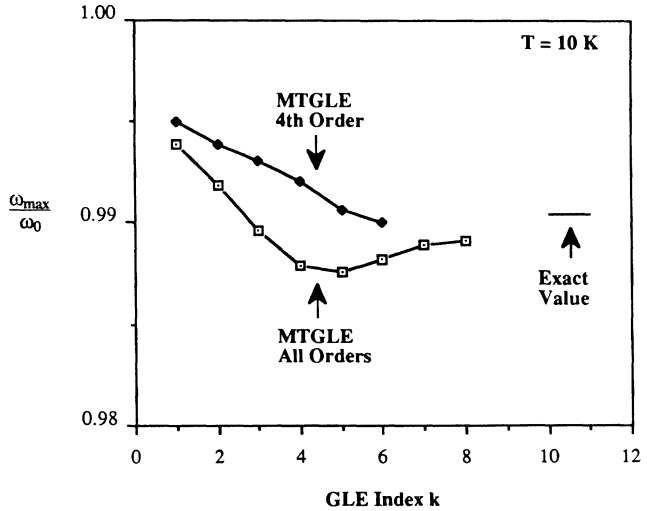

FIG. 11. Convergence of ω_{max} at $T=10$ K as a function of GLE index k. The Hamiltonian parameters are given in the text. The MTGLE calculations are carried out to fourth order and to all orders in the coupling constant. The predicted value is taken from Eq. (8).

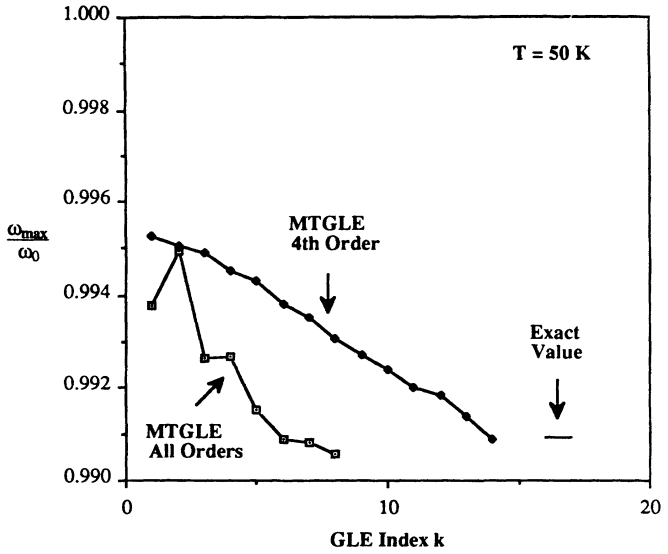

FIG. 12. Same as Fig. 11 with $T=50$ K.

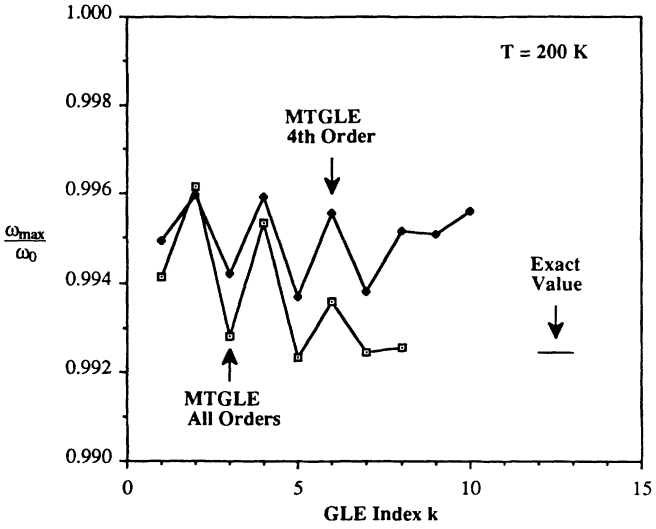

FIG. 14. Same as Fig. 11 with $T=200$ K.

verge toward the exact value at all temperatures, although the convergence is slower for ω_{max} than for the relaxation time τ.

For a MTGLE fourth-order calculation of ω_{max}, satisfactory convergence is not found, although at lower temperatures the value of ω_{max} calculated at the largest GLE index k is close to the exact value.

These results for ω_{max} contrast with results reported in I for the L-alanine parameter regime. In that case there was no significant change in going from a fourth-order MTGLE calculation to an all-orders calculation. This difference can be understood by noting that the coupling constant $\bar{\chi}$ appears quadratically in leading terms. Thus, although the single vibron frequency ω_0 has increased by a factor of approximately 30 in going from $\hbar\omega_0=60$ to 1665 cm^{-1}, the nonlinear coupling has increased by a factor of more than 1000 in going from $\bar{\chi}^2=(0.3\ cm^{-1})^2$ to $(10\ cm^{-1})^2$. We conclude that in the α-helix parameter regime care must be taken to ensure convergence with respect to the order to which the moments of $\dot{\chi}(t)$ are calculated.

Figures 16–20 show the full spectral density curves for $\dot{\chi}(t)$ for $T=10$, 50, 100, 200, and 300 K calculated by MTGLE theory from Eq. (33) using all-orders moments, the exact $\rho(\omega)$ calculated from Eq. (5), and the exact expressions for $\dot{\chi}(t)$ given by Eqs. (35), (36), and (40). There are small differences in the position of the center of the spectral line at 10 K, reflecting the difference between ω_{max} for the exact and MTGLE all-orders theories shown in Fig. 11. In all other cases the position and shape of the

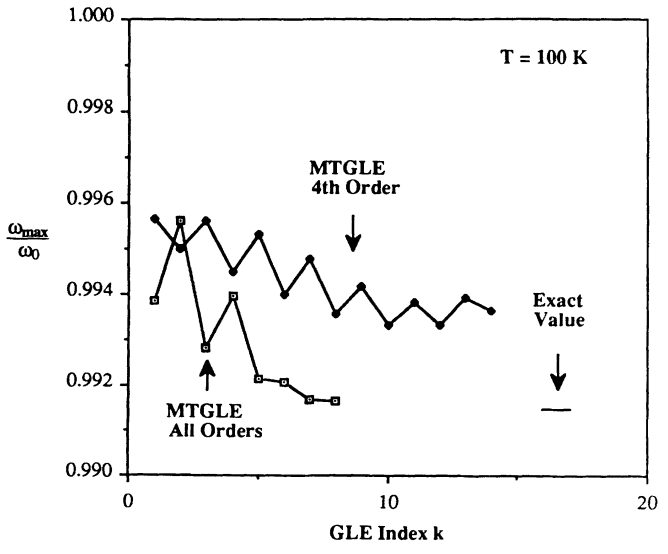

FIG. 13. Same as Fig. 11 with $T=100$ K.

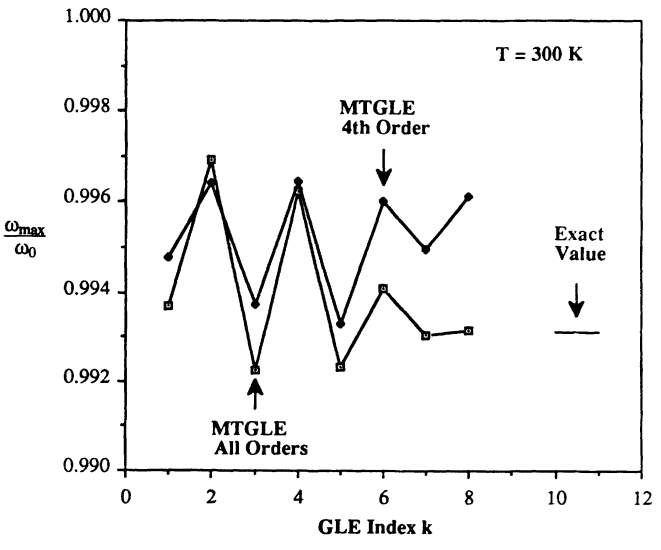

FIG. 15. Same as Fig. 11 with $T=300$ K.

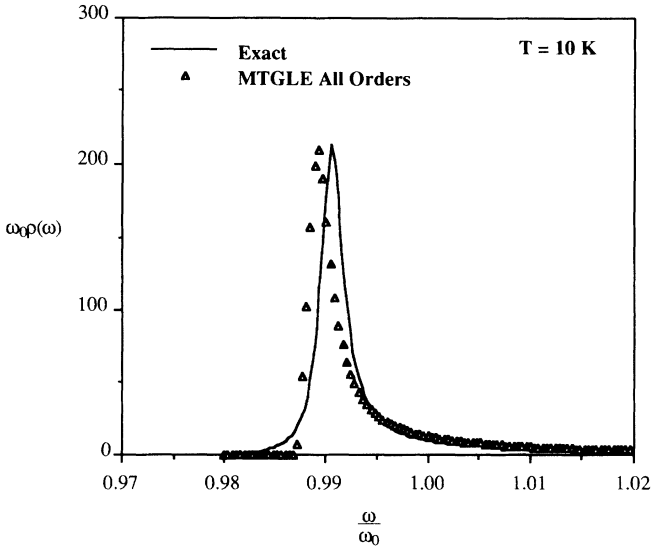

FIG. 16. Spectral density $\rho(\omega)$ as a function of ω at $T=10$ K for the MTGLE calculation using short-time derivative computed to all orders in the coupling constant and for exact theory.

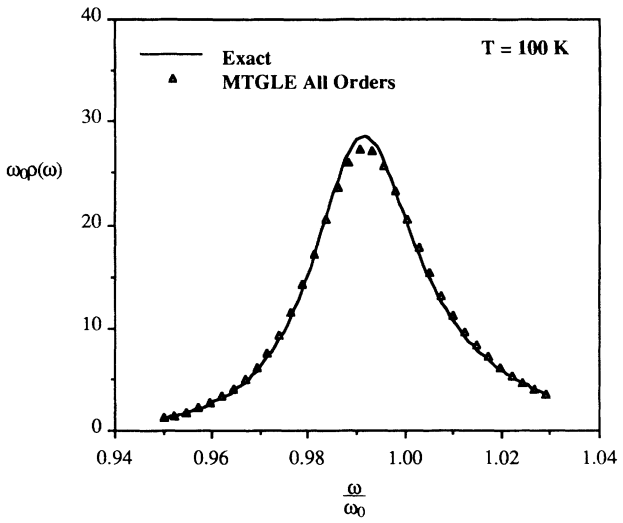

FIG. 18. Same as Fig. 16 with $T=100$ K.

spectral density curves calculated by MTGLE theory are in close agreement with the exact theory. This agreement extends to the MTGLE theory reproducing the substantially non-Lorentzian shape shown in Figs. 16–20.

C. Frequency modulation of $\dot{\chi}(t)$

The frequency of oscillation of $\dot{\chi}(t)$ is not constant, as is evident from the fact that the cosine functions in Eq. (36) contain the function $g(t)$. The time-dependent radian frequency of $\dot{\chi}(t)$, which we will denote by $\omega(t)$ and call the radian frequency per period, can be calculated by locating successive peaks in $\dot{\chi}(t)$ and computing $\omega(t)$ as $2\pi/\Delta t$) where Δt is the time difference between successive peaks. This can be done for the exact theory using Eqs. (35), (36), and (40) for MTGLE theory by first calculating $\rho(\omega)$ and then using its Fourier transform given by Eq. (6).

Figures 21–25 show $\omega(t)$ as a function of time calculated from the exact and MTGLE all-orders theories. The MTGLE fourth-order results are not very reliable, as mentioned above, and have been omitted for clarity. The general course of these curves is as follows. The time-dependent frequency $\omega(t)$ starts at ω_{e_0} as it must according to the definition of ω_{e_0} and Eq. (22). It then decreases sharply over many cycles to a value of $\omega(t)$ close to $\omega_{\max}$ given by Eq. (8). This sharp descent represents an initial contraction of the lattice about the vibron oscillator, and it is remarkable how well MTGLE theory reproduces the exact theory in this region. Following the sharp descent, $\omega(t)$ calculated from the exact theory shows small oscilla-

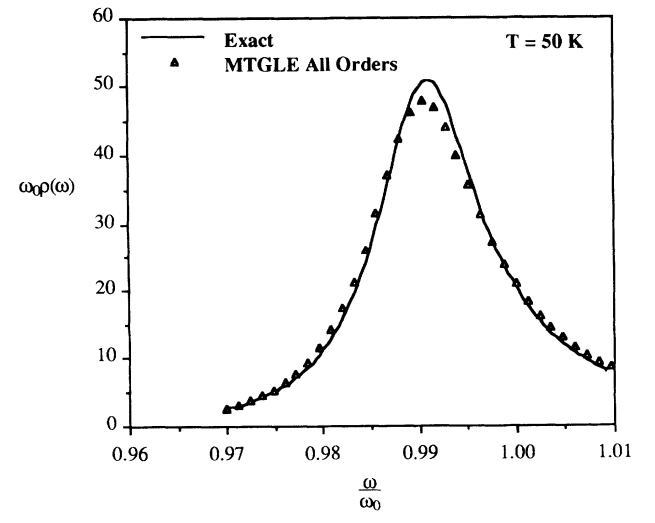

FIG. 17. Same as Fig. 16 with $T=50$ K.

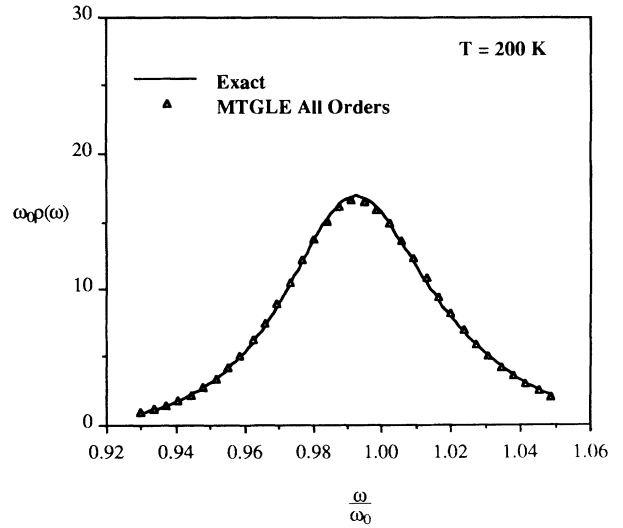

FIG. 19. Same as Fig. 16 with $T=200$ K.

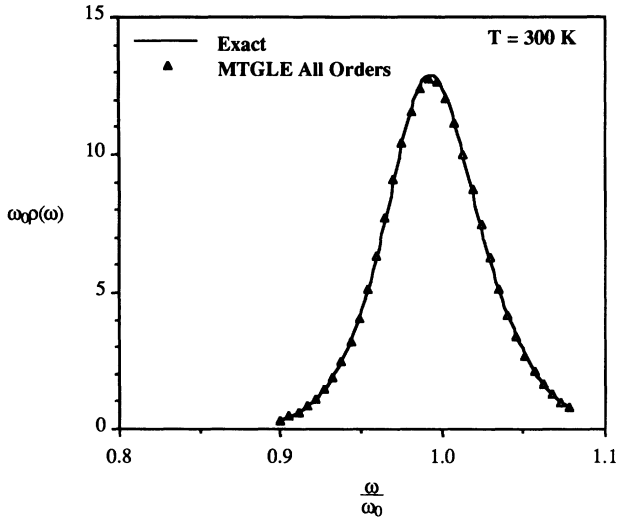

FIG. 20. Same as Fig. 16 with $T=300$ K.

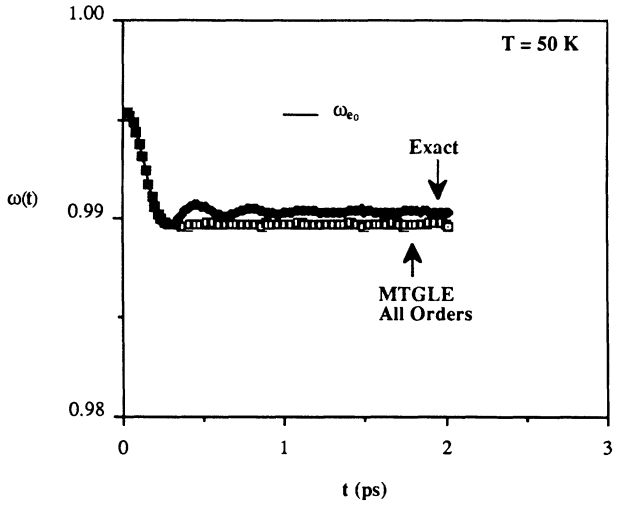

FIG. 22. Same as Fig. 21 with $T=50$ K.

tions about $\omega_{\max}$ and asymptotically approaches $\omega_{\max}$ after a few cycles of the radian frequency ω_a. In this same region $\omega(t)$ calculated from MTGLE theory flattens out at a value somewhat below $\omega_{\max}$. Considering the detailed nature of this test of MTGLE theory in the α-helix parameter regime, it is clear that MTGLE theory reproduces the exact results in a very satisfactory way. In Figs. 22–25 it should be noted the the calculation has been cut off in time at a point where t is approximately 4τ and the modulus of $\dot{\chi}(t)$ has become small and $\omega(t)$ is no longer of significance.

The failure of MTGLE theory to reproduce the oscillations in $\omega(t)$ found from the exact theory is of considerable theoretical interest. In I we showed that MTGLE theory gives an accurate representation of the first heat bath function $\theta_1(t)$ out to a time not less than

$$t=k\frac{\omega_e}{\omega_c^2}\ , \tag{47}$$

where k is the maximum available GLE index. If, for example, we use values for ω_e and ω_c given in the Appendix for $T=50$ K, we find $t=0.0289k$ ps. For a value of $k=8$ as the maximum available for the all-orders calculation, $t=0.23$ ps. We thus expect the MTGLE calculation to reproduce faithfully the exact calculations out to 0.25 ps, as it does. To reproduce the oscillations in $\omega(t)$ would require values of k out to about $k=30$, which is not computationally possible at present. Nevertheless, the MTGLE result for the redshift of the natural frequen-

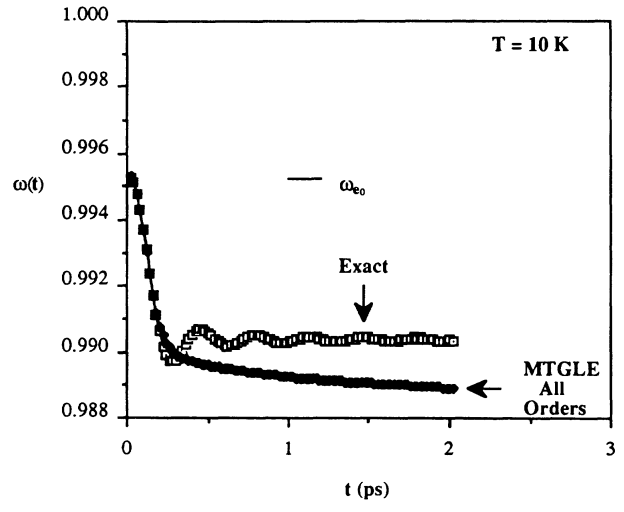

FIG. 21. Time-dependent radian frequency of $\dot{\chi}(t)$ as a function of time calculated according to the exact and MTGLE all-orders theories at $T=10$ K. The Hamiltonian parameters are given in the text. The value of the Einstein frequency ω_{e_0} is shown by a straight line, which is labeled.

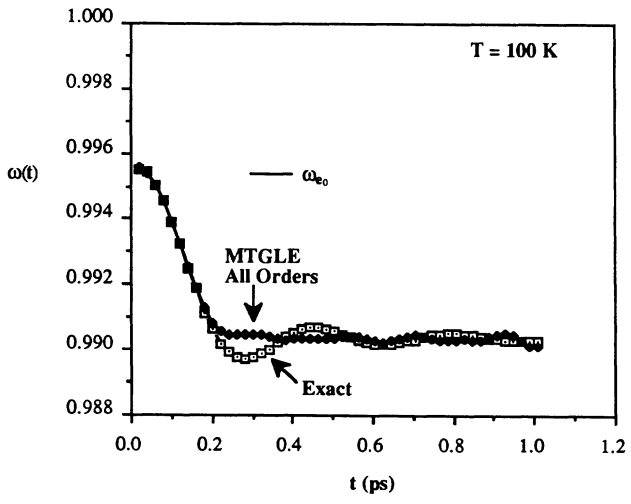

FIG. 23. Same as Fig. 21 with $T=100$ K.

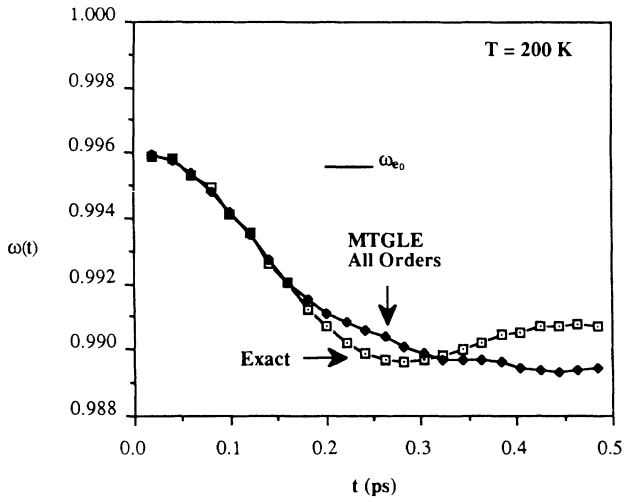

FIG. 24. Same as Fig. 21 with $T=200$ K.

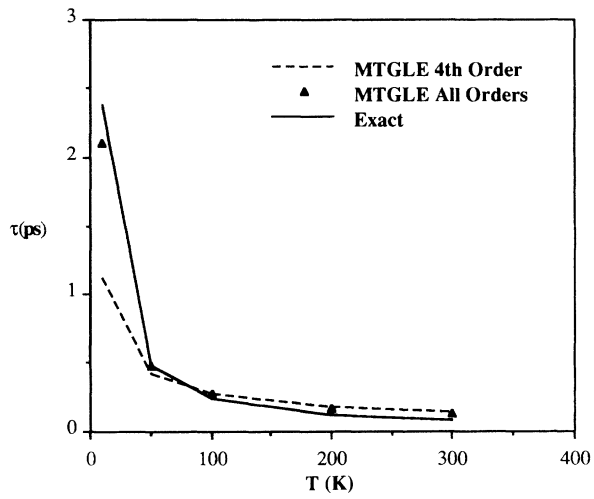

FIG. 26. Lifetime τ in ps as a function of temperature. The Hamiltonian parameters are given in the text. The MTGLE calculations are carried to fourth order and to all orders in the coupling constant.

cy ω_0 of the vibron oscillator is accurate in most cases to about 10% out to very long times. We emphasize again that this is a very stringent test of MTGLE theory in this parameter regime.

D. Relaxation time and resonant frequency as a function of temperature

The results of Secs. IV A and IV B can be seen from another perspective by plotting τ and $\omega_{\max}$ against temperature. In Fig. 26 we show τ as a function of temperature calculated from MTGLE theory using fourth-order and all-orders moments and also calculated from the exact theory. It can be seen that the agreement between the exact and all-orders MTGLE theories is extremely good with a small difference at the lowest temperature. The MTGLE results using fourth-order moments is also in reasonably good agreement with the two other calculations except for significant disagreement at 10 K. This reemphasizes that in the α-helix parameter regime the use of fourth-order moments is only marginally acceptable.

Figure 27 shows $\omega_{\max}$ plotted against temperature for the MTGLE theory using fourth-order and all-orders moments and also calculated from the exact theory. The story here is nearly the same for the exact and all-orders MTGLE theories which show good agreement except for the lowest temperature. The results using fourth-order moments in MTGLE theory by way of contrast are in poor agreement at most temperatures and emphasizes once again that the use of fourth-order moments for cal-

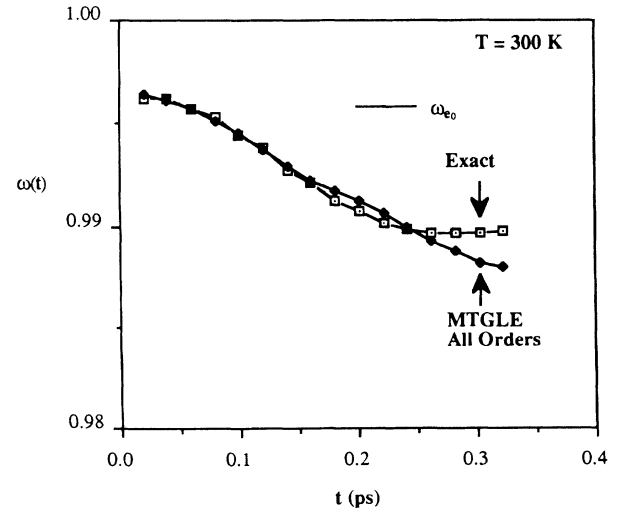

FIG. 25. Same as Fig. 21 with $T=300$ K.

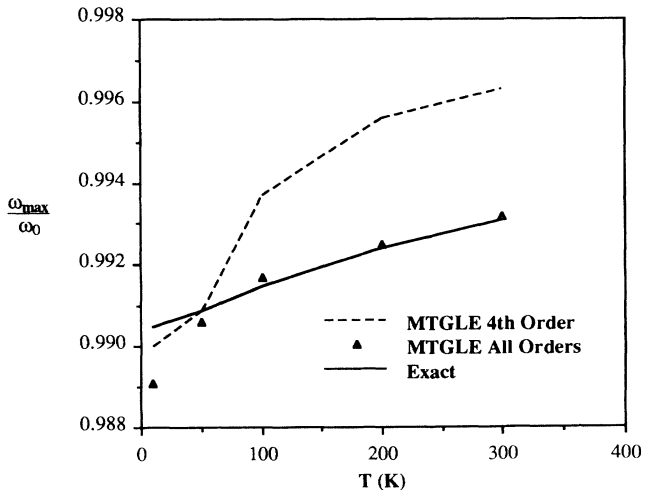

FIG. 27. $\omega_{\max}$ as a function of temperature. The Hamiltonian parameters are given in the text. The MTGLE calculations are carried to fourth order and to all orders in the coupling constant.

culating the resonant frequency of the spectral density curves is unacceptable.

V. SUMMARY AND CONCLUSIONS

In a previous paper (I), we have developed an approach to quantum molecular-time-scale generalized-Langevin-equation (MTGLE) theory and applied it successfully to calculating the spectral linewidth and redshift of a single vibron oscillator coupled to a linear chain of molecules comprising a phonon heat bath. We used the Davydov Hamiltonian because an exact solution was available for comparison with MTGLE theory. The Hamiltonian parameters used in I were in the range appropriate for coupled vibrational systems in molecular crystals such as L-alanine.

In this paper we extend the MTGLE and exact calculations of the same system to the parameter range appropriate to the coupling of intramolecular carbon-oxygen amide I stretching modes with low-frequency acoustic phonons in the α-helix. This represents a 30-fold increase in frequency of the vibron oscillator and a 1000-fold increase in the square of the nonlinear coupling constant. We have computed curves of the time evolution of the modulus of the correlation function $\dot{\chi}(t)$ by MTGLE theory which closely match results of the exact theory at temperatures ranging from 10 to 300 K. We have also calculated the time-dependent frequency $\omega(t)$ of $\dot{\chi}(t)$ and found satisfactory agreement with the exact theory.

In this parameter regime we find two significant differences from the previous calculations carried out in the L-alanine parameter regime, both related to computational problems. MTGLE theory depends on computing a large number of moments of the spectral density $\rho(\omega)$ associated with $\dot{\chi}(t)$. In I we were able to calculate moments to fourth order in the coupling constant and to all orders and found that the theory was insensitive to small differences between the fourth-order and all-order moments. This was an advantage because of the greater ease of calculating fourth-order moments and because more than nine moments could be calculated. In the present case we find there are substantial differences between the fourth-order and all-orders MTGLE calculations, and the fourth-order calculations do not give very satisfactory results.

The second difference is that it has not as yet been possible to calculate as many all-orders moments for the α-helix parameter regime as was possible for the L-alanine parameter regime. This implies that the first heat bath function $\theta_1(t)$ is only known accurately to shorter times and shows up in less accurate values for the redshift of the spectral density function and time-dependent frequency of $\omega(t)$. The overall conclusion, however, is that MTGLE theory is capable of calculating accurate linewidths (or relaxation times) and satisfactory redshifts for a wide range of temperatures in the α-helix parameter regime if the spectral moments are calculated to sufficient accuracy.

APPENDIX

In this appendix we describe a procedure to determine the constants ω_e and ω_c in Eq. (25). The need for this arose because the method described in I was unstable in the α-helix parameter regime and typically yielded oscillatory behavior for $\rho_1^*(\omega)$ in Eq. (27). We note that $\rho_1^*(\omega)$ is determined by fixing ω_e and ω_c and computing the coefficients α_k such that $\alpha_1=1$ and the other $2N-1$ coefficients satisfy the time derivative relationship in Eq. (20) for $m=1$. Further details of this calculation are provided in I. Our strategy herein is to carry out a Metropolis Monte Carlo walk for the parameters ω_e and ω_c such that certain features of $\rho_1^*(\omega)$ are optimized. These features are obtained as follows: We first note that $\rho_1^*(\omega)$ has band edges at $(\omega_e^2-2\omega_c^2)^{1/2}$ and $(\omega_e^2+2\omega_c^2)^{1/2}$. We tessellate this frequency range into equal-sized partitions with on the order of 100 partitions. At each partition point, which we label ω_i, we compute $\rho_1^*(\omega_i)$. Using these discretized values, we determine first the number of peaks P in the function. Second, we accumulate the area under the curve of $\rho_1^*(\omega)$ in regions where $\rho_1^*(\omega_i)<0$ by multiplying the magnitude of $\rho_1^*(\omega_i)$ times the partition width $\Delta\omega$. Thus, letting A be the accumulated area, we have

$$A=\sum_i |\rho_1^*(\omega_i)|\Delta\omega \ , \tag{A1}$$

for $\rho_1^*(\omega_i)<0$. Our goal in the Monte Carlo walk is to reduce the number of peaks P and the area A. Note that both of these quantities are positive definite.

Our Monte Carlo procedure uses the jump algorithms

$$\omega_e^{\text{new}}=\omega_e^{\text{old}}+\delta_e(\mathcal{R}-\tfrac{1}{2}) \tag{A2}$$

and

$$\omega_c^{\text{new}}=\omega_c^{\text{old}}+\delta_c(\mathcal{R}-\tfrac{1}{2}) \ , \tag{A3}$$

where δ_e and δ_c are jump distances and $\mathcal{R}$ is a uniformly distributed random number between 0 and 1. We accept or reject a given jump according to the following procedure: We compute the optimization function ϕ as

$$\phi=P+A \ . \tag{A4}$$

We calculate the ratio R_a as

$$R_a=\exp\left[\frac{\phi^{\text{old}}-\phi^{\text{new}}}{T_A}\right] , \tag{A5}$$

where T_A is a specified "annealing temperature." If R_a is greater than 1 or greater than a random number $\mathcal{R}$, then we accept the move. At the present time we carry out this simulated annealing by interactively changing δ_e, δ_c , and T_A after a specified number of attempted jumps until we are satisfied with the value of ϕ. The values of ω_e and ω_c determined and used in this paper are given in Table I.

In I we defined not only the approximation $\rho_1^*(\omega)$ to $\rho_1(\omega)$ but also $\rho_1'(\omega)$. The function $\rho_1'(\omega)$ is a point or "stick spectrum" approximation to $\rho_1(\omega)$. We refer to Eq. (80) of I for specific details of the approximation. As

TABLE I. Values of ω_e and ω_c as a function of temperature.

T (K)	$\left(\frac{\omega_e}{\omega_0}\right)^2$	$\left(\frac{\omega_c}{\omega_0}\right)^4$
	MTGLE fourth order	
10	1.015 439	0.010 957
50	1.001 230	0.063 489
100	0.927 619	0.114 576
200	1.075 238	0.106 430
300	1.072 099	0.097 728
	MTGLE all orders	
10	1.350 774	0.035 389
50	1.069 742	0.012 896
100	1.057 660	0.019 361
200	1.049 280	0.033 653
300	1.060 772	0.041 796

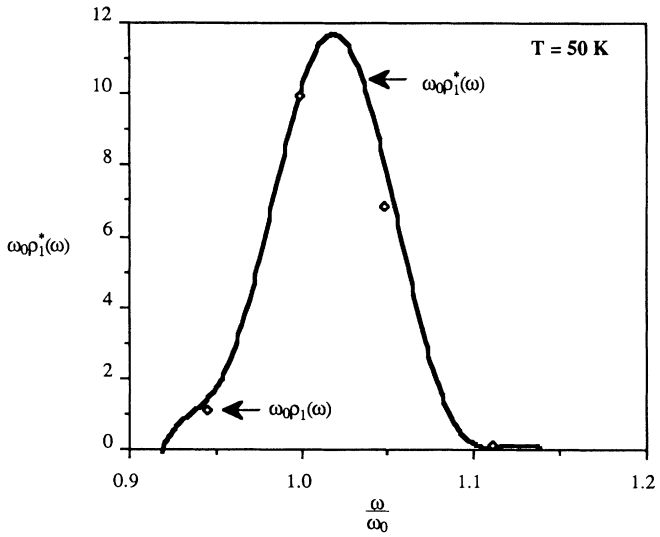

FIG. 28. Comparison of $\rho_1^*(\omega)$ and $\rho_1^*(\omega)$ for $T=50$ K.

we pointed out in I, agreement between $\rho_1^*(\omega)$ and $\rho_1'(\omega)$ typically led to well-behaved results. To show the level of this agreement for the α-helix parameter regime, we plot $\rho_1^*(\omega)$ and $\rho_1'(\omega)$ in Fig. 28 for $T=50$ K using MTGLE all-orders theory. The agreement is manifest. Similar agreement is found at $T=10$, 100, 200, and 300 K.

Two points should be made in conclusion. First, the final approximate $\rho_1^*(\omega)$, which we obtain correctly, fits the first $2N-1$ moments of $\rho_1(\omega)$ and is normalized. This is ensured by our computation of the α_k coefficients. Second, as we pointed out in I, it does not matter how one determines ω_e and ω_c. On the other hand, ω_e and ω_c should be chosen in such a way as to optimize convergence relative to the GLE index k. The method represented here focuses on choosing ω_e and ω_c such that $\rho_1^*(\omega)$ has the smallest number of peaks or oscillations as possible and such that regions where $\rho_1^*(\omega)<0$ are reduced. This procedure clearly optimally smooths $\rho_1^*(\omega)$ so that the weights in each frequency interval $\Delta\omega$ are as uniform as possible while still satisfying the constraints of fitting the first $2N-1$ moments of $\rho_1(\omega)$ and normalization. The spectral density therefore approximates a distribution of maximum entropy as shown by Levine.[19] We continue to look for better ways to determine ω_e and ω_c.

[1]A. S. Davydov and N. I. Kislukha, Phys. Status Solidi B **59**, 465 (1973).
[2]A. S. Davydov and N. I. Kislukha, Zh. Eksp. Teor. Fiz. **71**, 1090 (1976) [Sov. Phys. JETP **44**, 571 (1976)].
[3]A. S. Davydov, Phys. Scr. **20**, 387 (1979).
[4]S. Takeno, Prog. Theor. Phys. **69**, 1798 (1983); **71**, 395 (1984); **73**, 853 (1985).
[5]A. M. Clogston and H. K. McDowell, Phys. Rev. B **44**, 4978 (1991).
[6]G. Careri, U. Buontempo, F. Galluzzi, A. C. Scott, E. Gratton, and E. Shyamsunder, Phys. Rev. B **30**, 4689 (1984).
[7]C. T. Johnson and B. I. Swanson, Chem. Phys. Lett. **114**, 547 (1985).
[8]G. B. Blanchet and C. R. Fincher, Jr., Phys. Rev. Lett. **54**, 1310 (1985).
[9]A. C. Scott, E. Gratton, E. Shyamsunder, and G. Careri, Phys. Rev. B **32**, 5551 (1985).
[10]A. Tenenbaum, A. Campa, and A. Giansanti, Phys. Lett. A **121**, 126 (1987).
[11]A. Campa, A. Giansanti, and A. Tenenbaum, Phys. Rev. B **36**, 4394 (1987).
[12]A. Migliori, P. M. Maxton, A. M. Clogston, E. Zirngiebl, and M. Lowe, Phys. Rev. B **38**, 13 464 (1988).
[13]S. A. Adelman, Adv. Chem. Phys. **44**, 143 (1980).
[14]S. A. Adelman, Adv. Chem. Phys. **53**, 61 (1983).
[15]D. W. Brown, K. Lindenberg, and B. J. West, J. Chem. Phys. **84**, 1574 (1986).
[16]D. W. Brown, K. Lindenberg, and B. J. West, J. Chem. Phys. **87**, 6700 (1987).
[17]H. K. McDowell and A. M. Clogston (unpublished).
[18]H. K. McDowell, J. Chem. Phys. **87**, 4859 (1987).
[19]R. D. Levine, Adv. Chem. Phys. **47**, 239 (1981).
[20]H. K. McDowell, J. Chem. Phys. **93**, 6723 (1990).